LASER INTERFEROMETER GRAVITATIONAL WAVE OBSERVATORY
- LIGO -
CALIFORNIA INSTITUTE OF TECHNOLOGY
MASSACHUSETTS INSTITUTE OF TECHNOLOGY

| **Technical Note** | **LIGO-T22xxxxx–** | 2023/07/25 |
|---|---|---|

# Towards Improved Length Sensing and Control: Report 1

Deven Bowman

**California Institute of Technology**
**LIGO Project, MS 18-34**
**Pasadena, CA 91125**
Phone (626) 395-2129
Fax (626) 304-9834
E-mail: info@ligo.caltech.edu

**Massachusetts Institute of Technology**
**LIGO Project, Room NW22-295**
**Cambridge, MA 02139**
Phone (617) 253-4824
Fax (617) 253-7014
E-mail: info@ligo.mit.edu

**LIGO Hanford Observatory**
**Route 10, Mile Marker 2**
**Richland, WA 99352**
Phone (509) 372-8106
Fax (509) 372-8137
E-mail: info@ligo.caltech.edu

**LIGO Livingston Observatory**
**19100 LIGO Lane**
**Livingston, LA 70754**
Phone (225) 686-3100
Fax (225) 686-7189
E-mail: info@ligo.caltech.edu

http://www.ligo.caltech.edu/

# Contents

# 1 Introduction

Gravitational waves are distortions in spacetime produced by accelerating masses. Their existence was predicted over 100 years ago with the development of general relativity and the first experimental observation was made on September 14, 2015 by the Laser Interferometer Gravitational Wave Observatory (LIGO) of gravitational waves produced by a merger of 2 black holes.[1].

The Advanced LIGO detector is a pair of Michelson interferometers in Washington State and Louisiana with 4km arms containing Faby-Perot cavities to increase sensitivity [4]. A diagram of the interferometer is shown in figure 1.

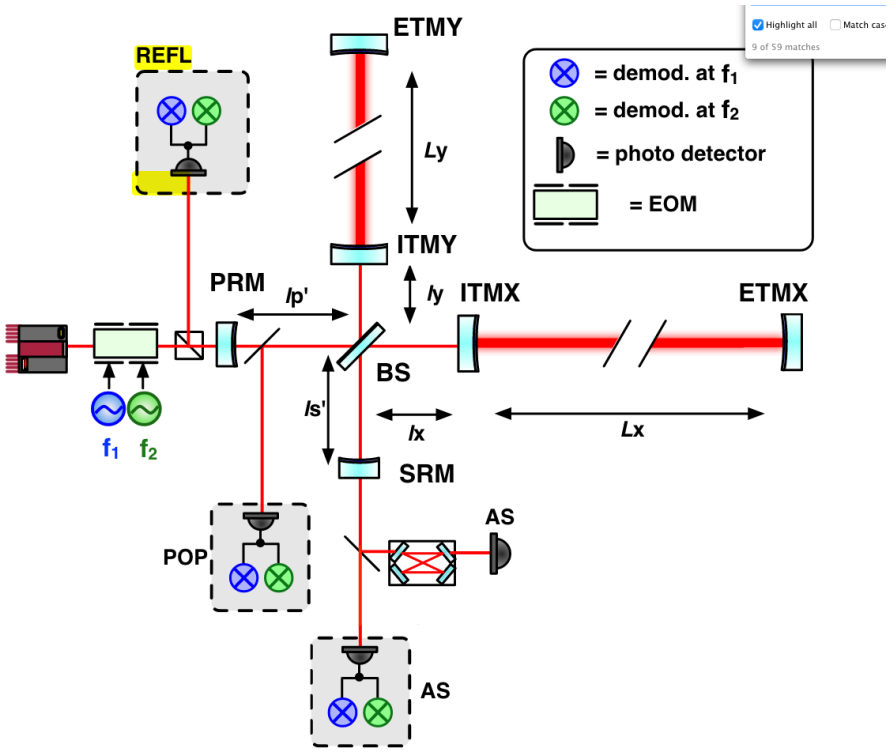


Figure 1: A diagram of one of the Advanced LIGO detectors [8]. REFL, POP, and AS denote collections of photodiodes measuring at DC and radio frequencies (RFPDS).

Gravitational waves cause the arms of the interferometer to lengthen and contract relative to each other as the wave propagates through the detector. This changes the path length for light traveling in each arm, producing a relative phase difference detectable through interference. Advanced LIGO's sensitivity curve is shown in figure 2.

There are many length degrees of freedom (DoF) that must be controlled for the detector to operate. The most important of these is DARM, defined below.

$$L_- = \frac{L_x - L_y}{2} \tag{1}$$

For the detector to operate, these length DoFs need to be controlled. This is achieved by deriving error signals from sensors around the detector. These error signals drive feedback

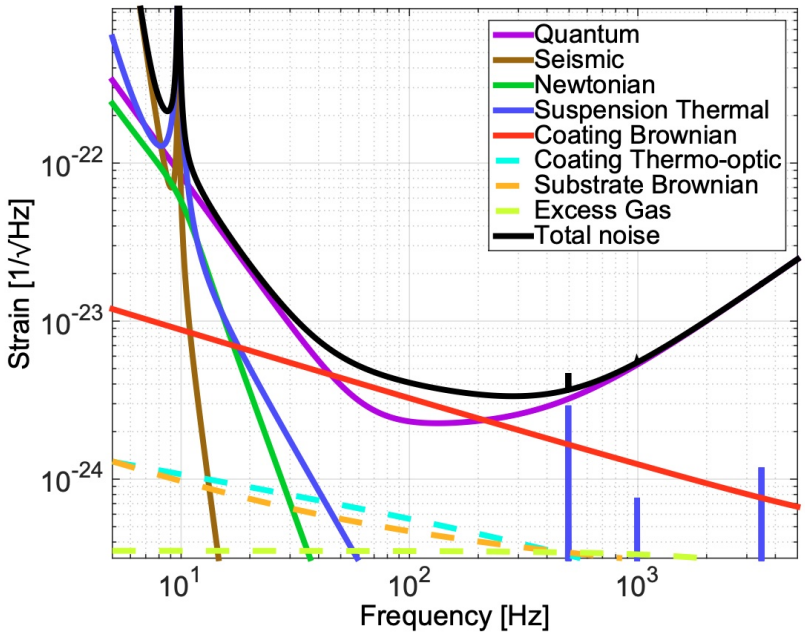


Figure 2: The sensitivity curve of Advanced LIGO [2]. Each line shows the amplitude spectral density of a noise source. The sum, in black, produces the predicted noise floor for advanced LIGO.

loops that keep the detector at its operating point. A block diagram of a simplified control loop for DARM is shown in figure 3. The plant of the control system is the suspension of the

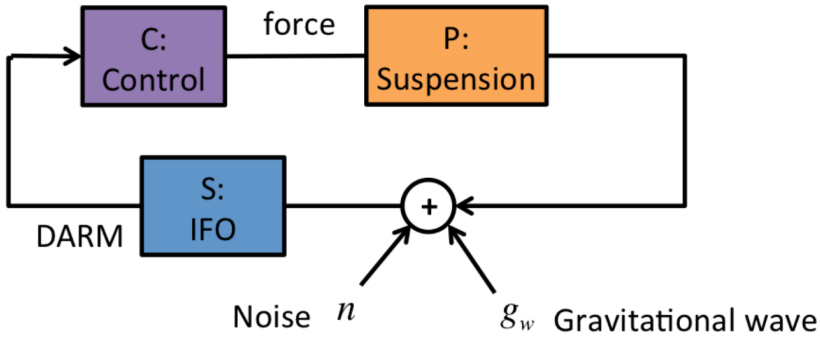


Figure 3: The control loop for DARM shown with the injection of displacement noise and gravitational wave signal [9].

mirrors. These are disturbed by the gravitational wave signal and noise causing additional displacement to the mirrors. The sensors converts this to an error signal for DARM and the control block uses the error signal to drive actuators that apply force to the mirrors to return them to the set point. The DARM signal can calculated from the open loop transfer functions.

$$DARM = \frac{S}{1 + CPS}(n + g_w) \tag{2}$$

This length control system is needed to stabilize the detector against displacement noise to maintain a linear response to fluctuations in its DoF. However, by controlling mirror motion

against displacements, the mirror motion due to gravitational wave signals is also suppressed. The gravitational wave signal is attained by applying the inverse of the closed loop transfer function from the displacement signal to DARM.

$$g_w = \frac{1 + \hat{C}\hat{P}\hat{S}}{\hat{S}} DARM \tag{3}$$

The hats on the inverse transfer functions indicate that they are models that must be measured for accurate readout of the signal.

The control system is a key part of the detectors function. Currently, there are more sensors with some coupling to the length DoFs than there are length DoFs. A linear system that uses the outputs of all of these detectors would be overdetermined. The current control techniques only employ a subset of the sensors to generate a determined system: equal numbers of detectors and sensors. This project will explore the potential benefits to the sensitivity of the detector from designing an overdetermined control system that can take advantage of noise correlations between the detectors to reduce the susceptibility of the control system to various noise inputs.

# 2 PRMI Configuration

We consider the simplified detector configuration of a Michelson interferometer with a power recycling cavity(PRMI). This is a simplification of the Advanced LIGO detector configuration since there are no Faby-Perot cavities in the detector arms and no signal recycling mirror after the anti-symmetric port of the beam splitter to form a signal recycling cavity. There are two important length DoFs in this configuration, MICH and PRCL, defined in equations 4 and 5 respectively based on length definitions in figure 1. MICH is the difference in the arm lengths and PRCL is the length of the power recycling cavity.

$$l_- = \frac{l_x - l_y}{2} \tag{4}$$

$$l_p = l'_p + \frac{l_x + l_y}{2} \tag{5}$$

# 3 PRMI Length Control System

A block diagram representing the general structure of the control system for MICH and PRCL is shown in figure 4. **C**, **P**, and **S** are the transfer functions for the controller/actuator, the mechanical plant of the length DoFs, and the sensors. $n_d$, displacement noise, represents forces on the optics which generate fluctuations in MICH and PRCL. $n_c$ represents noises that will be correlated in the sensors: noise in the laser frequency or amplitude for example. $n_s$ is noise that enters the loop through measurement and analog to digital conversion of the signals at each sensor. The purpose of the control system is to suppress the effects of $n_d$, but by closing the loop, $n_c$ and $n_s$ inject additional noise into MICH and PRCL. This is why care must be taken to generate the error signals for control. The current design of **M**,

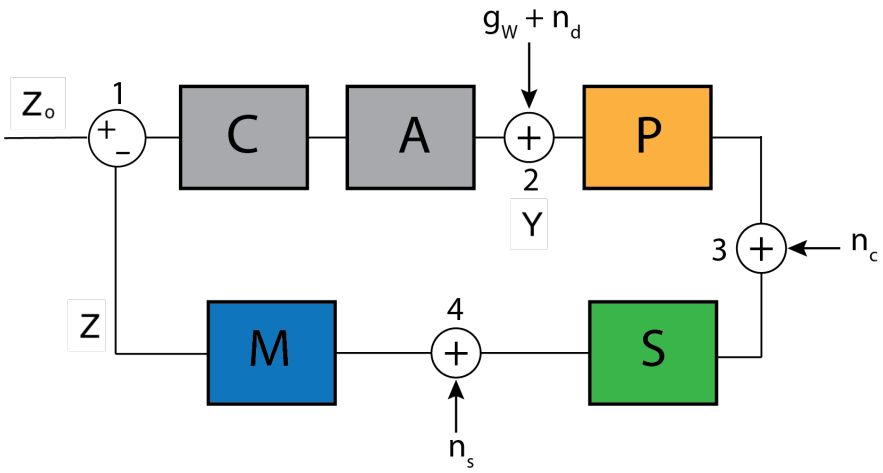


Figure 4: The a block diagram for the control loop for MICH and PRCL in the PRMI configuration is shown.

the mixing matrix, selects one sensor for each DoF to generate an error signal and discards the rest of the sensors. Currently, PRCL is sensed with a REFL photodiode demodulated at 11MHz and MICH is sensed by an AS photodiode demodulated at 55 MHz.

# 4 Mixing Matrix Optimization

In general, **M** can take a frequency dependent linear combination of a large collection of REFL, POP, and AS sensors. The goal is to use measurements of the open loop transfer functions in the control system and measurements of the noise in each sensor to solve for **M** that minimizes the total noise in $Y$.

## 4.1 Optimization Method

The mixing matrix will be optimized to reduce the power spectral density (PSD) of the noise on each DoF. To do this, we need to understand how noise powers are propagated through the feedback system to $Y$. The noise signals can be propogated to $Y$ with the following transfer functions.

$$\mathbf{T_{y,n_d}} = (\mathbf{I_{2x2}} + \mathbf{PCMS})^{-1}\mathbf{P} \tag{6}$$

$$\mathbf{T_{y,n_c}} = -(\mathbf{I_{2x2}} + \mathbf{PCMS})^{-1}\mathbf{PCMS} \tag{7}$$

$$\mathbf{T_{y,n_s}} = -(\mathbf{I_{2x2}} + \mathbf{PCMS})^{-1}\mathbf{PCM} \tag{8}$$

The first subscripts denotes the codomain of each transfer function, $Y$ in this case, and the second subscript denotes the domain, each noise source. The noise contribution to $Y$ from

$n_s$ can be calculated as follows.

$$n_s = (n_{s1}, \ldots, n_{sN})^T \tag{9}$$

$$Y_{n_s} = \mathbf{T_{y,n_s}}(n_{s1}, \ldots, n_{sN})^T = \begin{pmatrix} \alpha_{11} & \ldots & \alpha_{1N} \\ \alpha_{21} & \ldots & \alpha_{2N} \end{pmatrix} (n_{s1}, \ldots, n_{sN})^T \tag{10}$$

Then, up to a normalization factor, the PSD of $Y_{n_s}$ follows from the norm squared of $Y_{n_s}$. For the first component of $Y_{n_s}$, MICH, it is the following.

$$|y_{1,n_s}|^2 = y_{1,n_s} y_{1,n_s}^* = |\alpha_{11 n_s 1}|^2 + \alpha_{11} n_{s1} (\alpha_{12} n_s 2)^* + \ldots = \mathbf{T_{y,n_s,1}} \mathbf{\Sigma_{n_s}} \mathbf{T_{y,n_s,1}}^H \tag{11}$$

$\mathbf{T_{y,n_s,1}}$ is the first row of $\mathbf{T_{y,n_s}}$, $\mathbf{\Sigma_s}$ is the covariance matrix of the noises present in the sensor signals, and $X^H$ is the hermitian conjugate of $X$. Each row of these transfer functions contains the weights for a linear combination of noises. The covariance matrix acts as a bilinear form which maps these weights to a noise PSD. The total PSD for $Y$ is the quadrature sum of the contributions from $n_d$, $n_c$, and $n_s$.

## 4.2 Simulation

This analysis was carried out on a model of the control system. This simulation had 3 sensors and the following covariance matrices were used.

$$\mathbf{\Sigma_s} = \begin{pmatrix} 1.1 & 0.1 & 0.1 \\ 0.1 & 1.1 & 0.1 \\ 0.1 & 0.1 & 1.1 \end{pmatrix} \tag{12}$$

$$\mathbf{\Sigma_d} = \begin{pmatrix} 1.1 & 0.1 \\ 0.1 & 1.1 \end{pmatrix} \tag{13}$$

$\mathbf{\Sigma_s}$ includes $n_s$ and $n_c$ sources and $\mathbf{\Sigma_d}$ includes $n_d$. The plant was modeled as a diagonal matrix with $\frac{1}{f^2}$ on-diagonal terms to capture the general behavior of the pendulum suspension of the mirrors. $\mathbf{C}$ was then chosen such that $\mathbf{PC} = \frac{G}{f}\mathbf{I_{2x2}}$, a gain factor with $1/f$ dependence. They are written explicitly in the following equations.

$$\mathbf{P} = \begin{pmatrix} \frac{1}{f^2} & 0 \\ 0 & \frac{1}{f^2} \end{pmatrix} \tag{14}$$

$$\mathbf{C} = \begin{pmatrix} Gf & 0 \\ 0 & Gf \end{pmatrix} \tag{15}$$

The sensing matrix was taken to be a 3x2 matrix with random coefficients in (0,1). The amplitude spectral density (ASD) of $Y$, the square root of the PSD, was calculated with the method described and `scipy.optimize.minimze` was used to find the coefficients to minimize ASD at each frequency. The minimization only considered the ASD of $y_1$. A cost function that incorporates both $y_1$ and $y_2$ needs to be developed. The results are shown in figures 5 and 6. In figure 5, the ASD from the optimal mixing matrix is compared to the open loop displacement noise, $|\mathbf{P}n_d|$, and the ASD where $\mathbf{M}$ was chosen as the generalized inverse of $\mathbf{S}$. The open loop noise spectrum is $\frac{1}{f^2}$. With the control system on and $\mathbf{MS} = 1$,

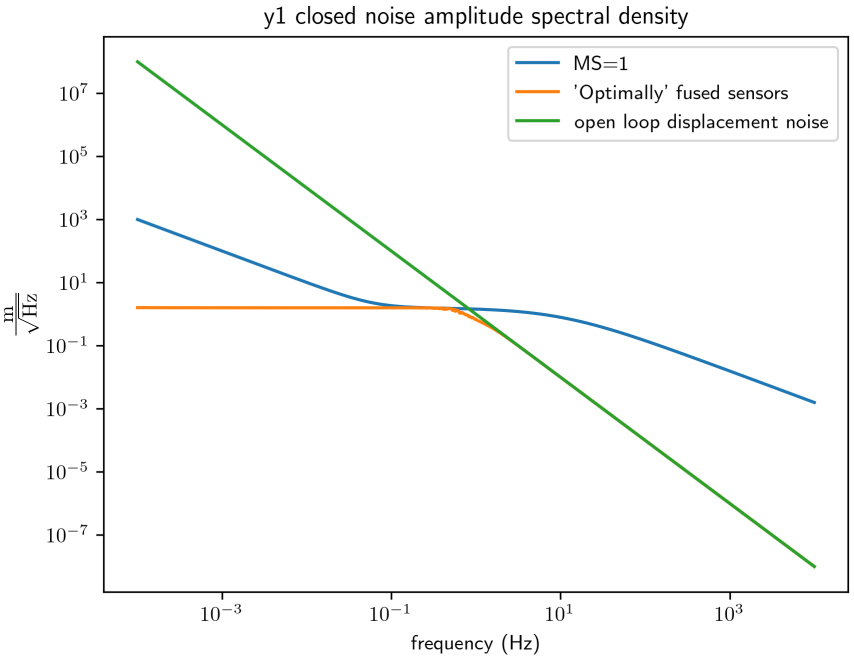


Figure 5: The ASD from a simulated control loop for MICH and PRCL. The open loop $n_d$ is plotted in green. The blue line is attained by choosing $\mathbf{M}$ to be the generalized inverse of $\mathbf{S}$. The optimized mixing matrix produced the orange curve.

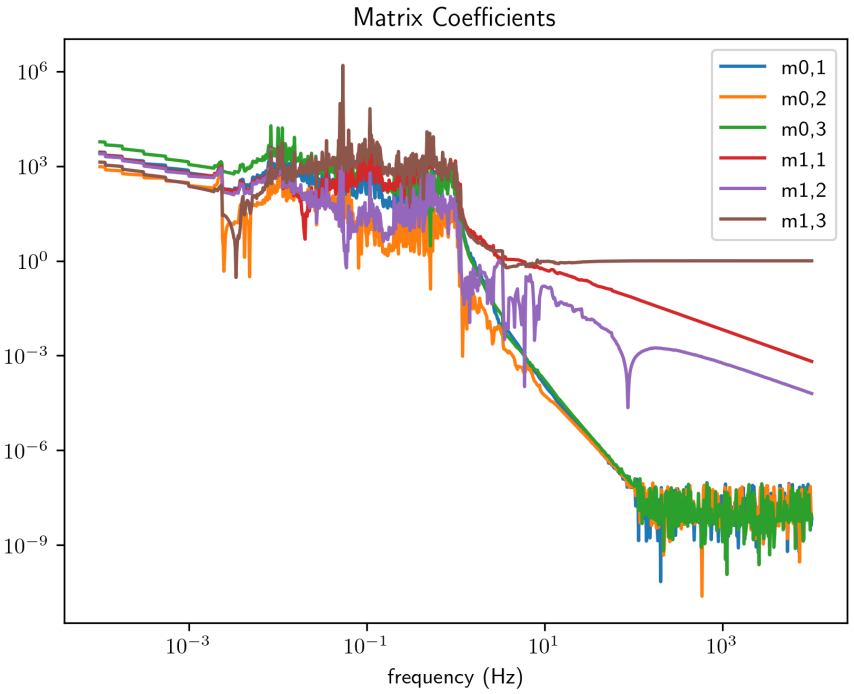


Figure 6: The coefficients of the optimal mixing matrix in figure 5 are graphed.

the displacement noise is suppressed until $\sim$ 1Hz where the magnitude of the displacement noise is comparable to the magnitude of the sensing noise. At high frequencies, the noise spectrum falls off as $\frac{1}{f}$ due to the choice of $\mathbf{C}$. With the optimized mixing matrix, the noise is suppressed to a flat spectrum at low frequencies and $\frac{1}{f^2}$ at high frequencies. Figure 6 shows that this is accomplished by large gain from all the coefficients at low frequencies and then filtering signals at $f \geq 1$ Hz. In practice, too much gain may make the system unstable so the actual performance is likely to be limited to a higher noise floor at low frequencies. The 1Hz transition frequency between the dominance of $n_d$ to $n_s + n_c$ is determined by the relative magnitudes of the noise sources and is thus arbitrary in the simulation presented. Measurements of real noises in the 40m prototype will elucidate the real transition frequency.

# 5 40m LIGO Prototype PRMI Measurements

While locked in the PRMI configuration, the sensing matrix $\mathbf{S}$ was measured as well as time series data from a collection of REFL and AS sensors. Spectral analysis of these time series will allow for the frequency dependent covariance matrices to be calculated. The mixing matrix optimization process assumed independent knowledge of $n_d$ from $n_s$ and $n_c$. In practice, all the noise contributions will appear in each sensor. An attempt to separate $n_d$ from the others will be made by fitting the noise spectrum to $\frac{A_0}{f^{-2}}$ at low frequencies where displacement noise is dominant and then subtracting this fitted spectrum from all frequencies to generate an estimate of $n_c + n_s$.

# 6 Next Steps

The measurements made at the 40m LIGO prototype will be analyzed to calculate an optimal mixing matrix. This can then be implemented during the next 40m PRMI lock to compare the performance. The current optimization method produces a frequency dependent matrix. To implement this, some parts of the digital control systems for the length sensing and control at the 40m will need to be modified. In addition, a stability analysis should be performed to understand if modifications need to be made to the fitted $\mathbf{M}$ to work in practice.

# References

[1] B. P. Abbot et al. (LIGO Scientific Collaboration and Virgo Collaboration). Observation of Gravitational Waves from a Binary Black Hole Merger. Phys. Rev. Lett., 116, 061102 (2016).

[2] L. Barsotti, S. Gras, M. Evans, P. Fritschel. The updated Advanced LIGO design curve. (2018)

[3] Aasi, J., Abadie, J., Abbott, B. et al. Enhanced sensitivity of the LIGO gravitational wave detector by using squeezed states of light. Nature Photon. 7, 613-619 (2013).

[4] LIGO Scientific Collaboration. Advanced LIGO. arXiv:1411.4547 (2014).

[5] Gilbert Grynberg, Alain Aspect, and Claude Fabre. Introduction to Quantum Optics. Chapter 5 (2010).

[6] Mark Fox. Quantum Optics An Introduction. Chapter 7 (2006).

[7] G. Venugopalan et al. Prototype Interferometry in the Era of Gravitational Wave Astronomy, Phys. Rev. A, 102, 023507 (2020)

[8] E. A. Quintero et al. Improving the Performance and Sensitivity of Gravitational Wave Detectors. Review of Scientific Instruments, 87, 065107 (2016)

[9] Brett Shapiro. Intro to Control Theory for LIGO People. Lecture 2, G1600726-v3.